Reversible Surface Reconstruction of Metal-Organic Frameworks for Durable Oxygen Evolution Reaction

Shulin Li, †[a, b, c] Zhaoxin Zhou, †[b] Jiahui Lia, [a] Yang Xiao, [a] Ye Yuan, [a] He Zhu, [b] Fengchao Cui,*[a] Xiaofei Jing,*[a] and Guangshan Zhu*[a]

[a.] *Key Laboratory of Polyoxometalate and Reticular Material Chemistry of Ministry of Education, Northeast Normal University, Changchun 130024, China.*

E-mail: jingxf100@nenu.edu.cn; zhugs@nenu.edu.cn

[b.] *School of Science and Engineering, The Chinese University of Hong Kong, Shenzhen 518172, China*

[c.] *School of chemistry, Chongqing Normal University, Chongqing 400000, China*

†These authors contributed equally to this work.

DFT calculations

We calculated the Gibbs free energy as function of reaction pathway of oxygen evolution reaction (OER) with spin-polarized DFT calculations using the Vienna ab initio Simulation Package (VASP 5.4.4). [1] The approach of estimating free energy for OER by DFT is based on the method proposed by Norskov et al. [2-3] Model of γ-NiOOH/Ni-BPM were constructed by loading a layer γ-NiOOH on Ni-BPM bulk structure.

Each system was geometry optimized using VASP and a 2×2×2 Gamma-centered *k*-point mesh. The OER process includes 4 steps,

$$* + \mathrm{OH}^- \rightarrow \mathrm{HO}* + e^- \qquad (1)$$

$$\mathrm{HO}* + \mathrm{OH}^- \rightarrow \mathrm{O}* + \mathrm{H_2O} + e^- \qquad (2)$$

$$\mathrm{O}* + \mathrm{OH}^- \rightarrow \mathrm{HOO}* + e^- \qquad (3)$$

$$\mathrm{HOO}* + \mathrm{OH}^- \rightarrow * + \mathrm{O_2} + \mathrm{H_2O} + e^- \qquad (4)$$

where * represents the active sites. The initial position of the HO*/O*/HOO* groups was placed perpendicular to the *ab* plane and along the *c* direction. Separate calculations indicated that the HO*/O*/HOO* groups cannot attach to the metal sites if they were placed along the *a* direction and perpendicular to the *bc* plane. The initial distance between O and each metal site was set to be 2.084 Å, the same as the Ni-O distance in bulk NiO. We calculated the binding energy of HO*, O* and HOO* for each system respectively. The Gibbs free energy ΔG of each OER step was calculated by

$$\Delta G = \Delta E + \Delta ZPE - T\Delta S + \Delta G_U \qquad (5)$$

where ΔE is the binding energy, ΔZPE is the zero-point energy correction, $T\Delta S$ is the entropy correction based on the vibrational entropy change at temperature T, and ΔG_U is energy correction due to the electrode potential *U*. The vibrational frequencies of the HO*/O*/HOO* groups were calculated by the configurations from the converged binding energy calculation. The $\Delta ZPE - T\Delta S$ term was then estimated using the vaspkit package at 298.15 K. [4] We did not compute the influence of pH since this would not differ among the set of materials we considered. The entropy corrections for adsorbates were also computed using vaspkit. [2, 4]

Table S1. The Ni-Ni distance and Ni-O bond length in Ni-BPM and NiOOH.

	Ni-BPM	*γ*-NiOOH	*β*-NiOOH
Ni-Ni (Å)	2.963	3.071	2.92
Ni-O (Å)	2.013	1.967	2.363

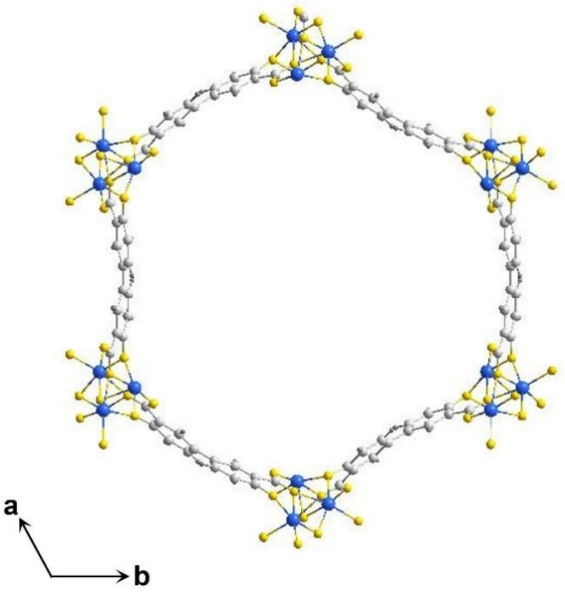

Fig. S1 Coordination environments of metal ions in Ni-BPM along *c* axis.

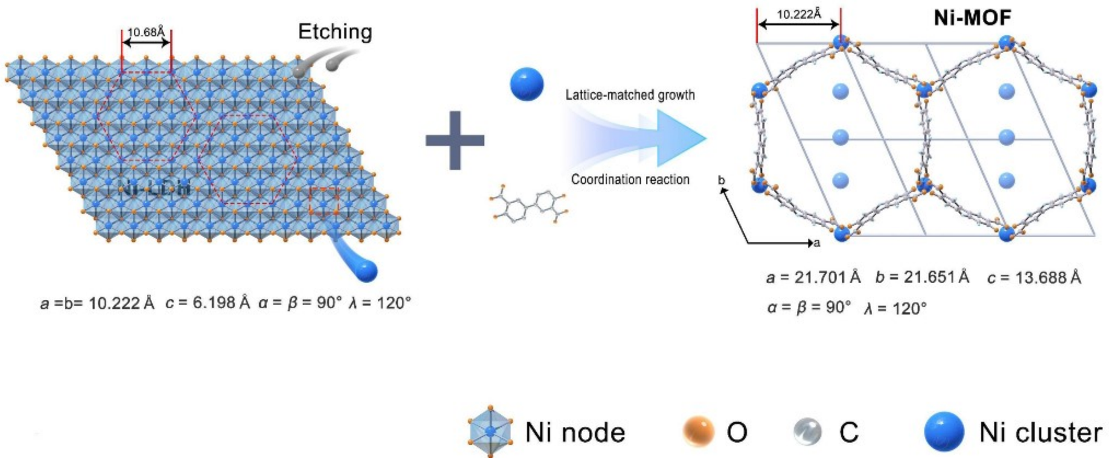

Fig. S2 Schematic illustration of lattice-matched template preparation of Ni-BPM/NF.

The cell parameters of Ni-LDH are as follows: a = 10.222 Å, b = 10.222 Å, c = 6.198 Å, and $\alpha = \beta = \gamma = 90.00°$. The cell parameters of Ni-BPM are as follows: a = 21.704 Å, b = 21.704 Å, c = 6.844 Å, and $\alpha = \beta = \gamma = 90.00°$. The above data indicates that the exposed (0 0 1) plane of Ni-BPM is matched to the (0 0 2) plane of Ni-LDH. Metal node in Ni-BPM (0 0 1) plane is linked to the adjacent node with the distance of 10.68 Å. A similar metal node distante should be kept in Ni-LDH (0 0 2) plane to allow Ni-BPM lattice-matched growth.

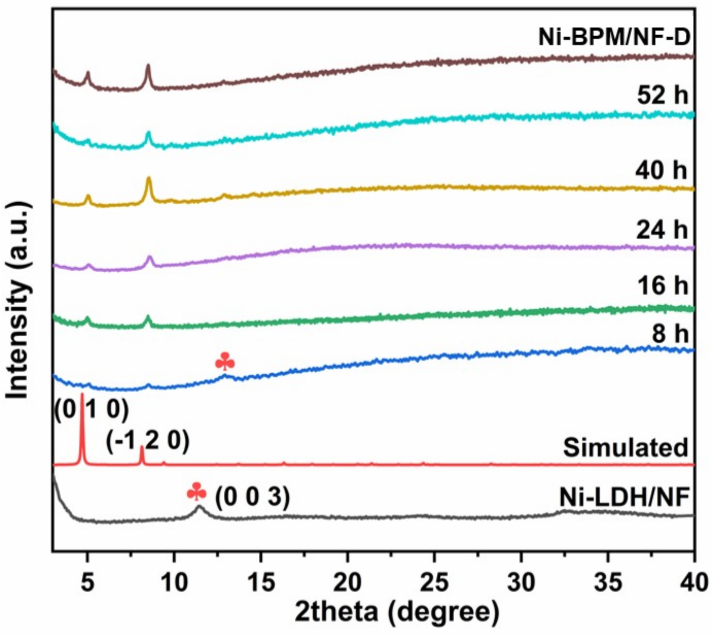

Fig. S3 XRD patterns of Ni-LDH/NF, Ni-BPM/NF-D and Ni-BPM/NF-x (x = 8, 16, 24, 40, 52 h), respectively.

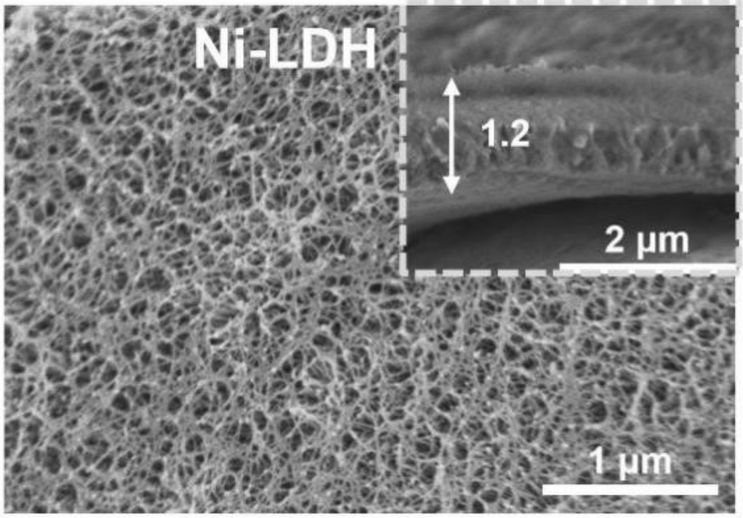

Fig. S4 SEM images of Ni-LDH/NF.

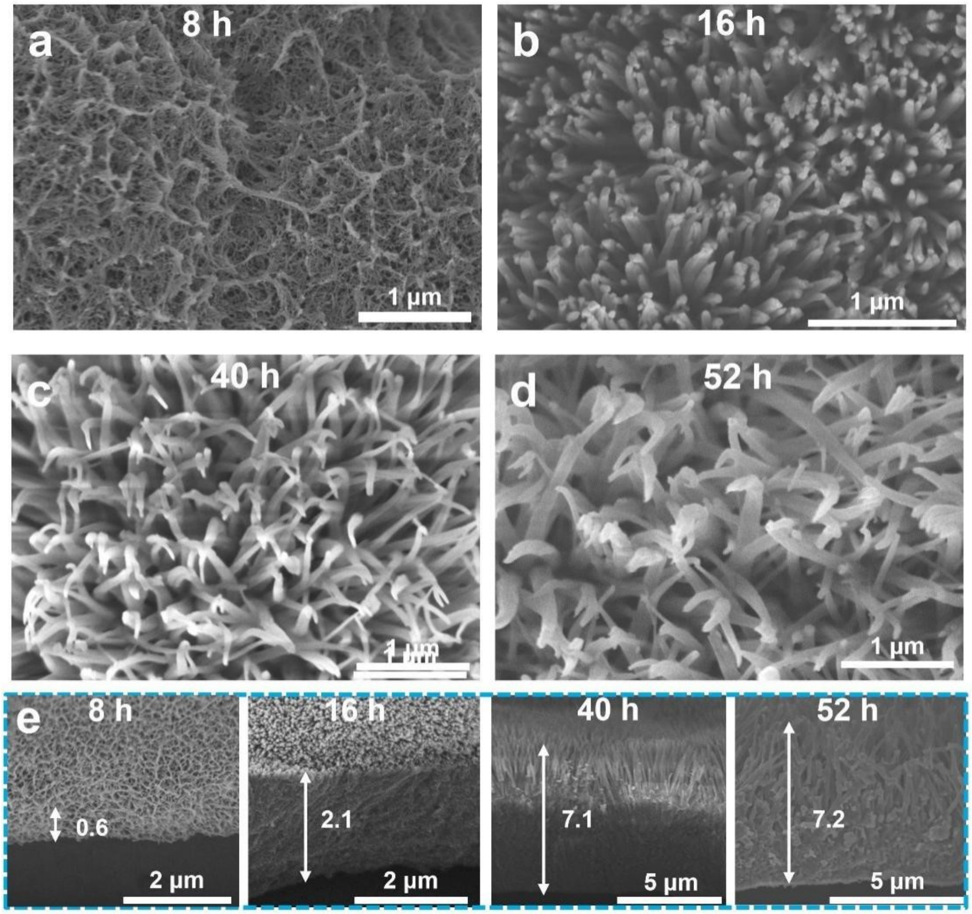

Fig. S5 SEM images of Ni-BPM/NF-x (x = 8, 16, 40, 52 h) respectively.

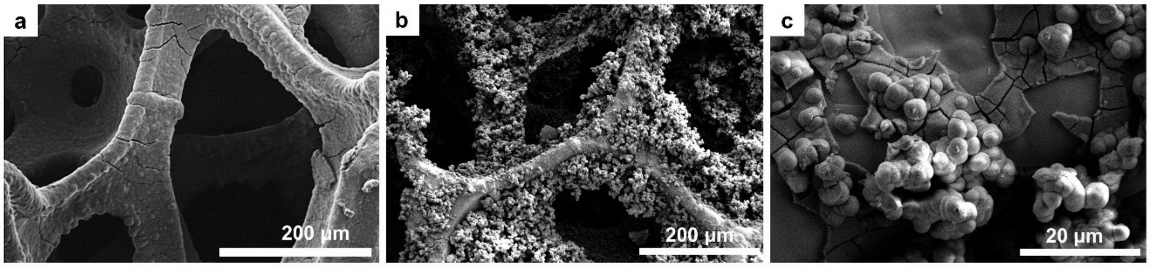

Fig. S6 SEM images of Ni-BPM/NF-24h (a) and Ni-BPM/NF-D (b, c).

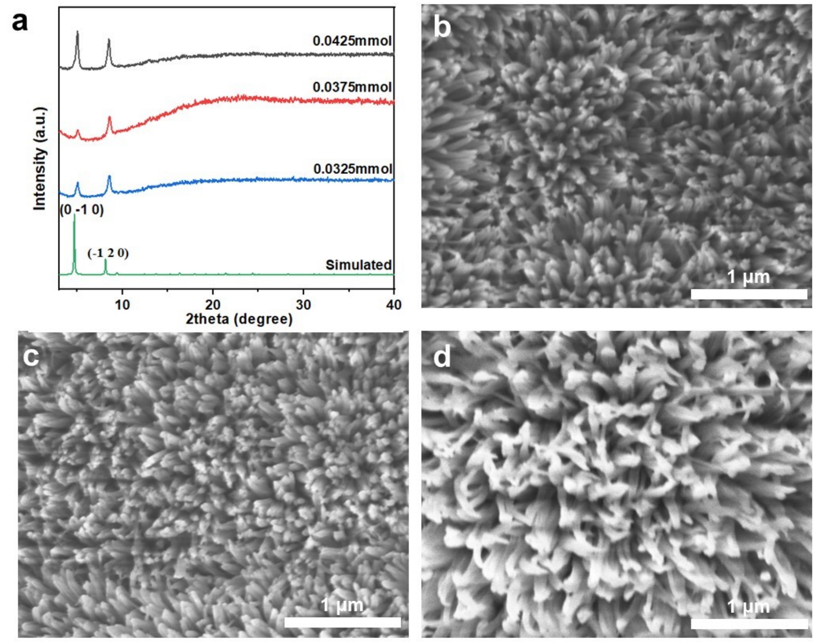

Fig. S7 XRD patterns (a) and SEM images of different ligand concentration, including 0.0325 mmol (b), 0.0375 mmol (c), 0.0425 mmol (d).

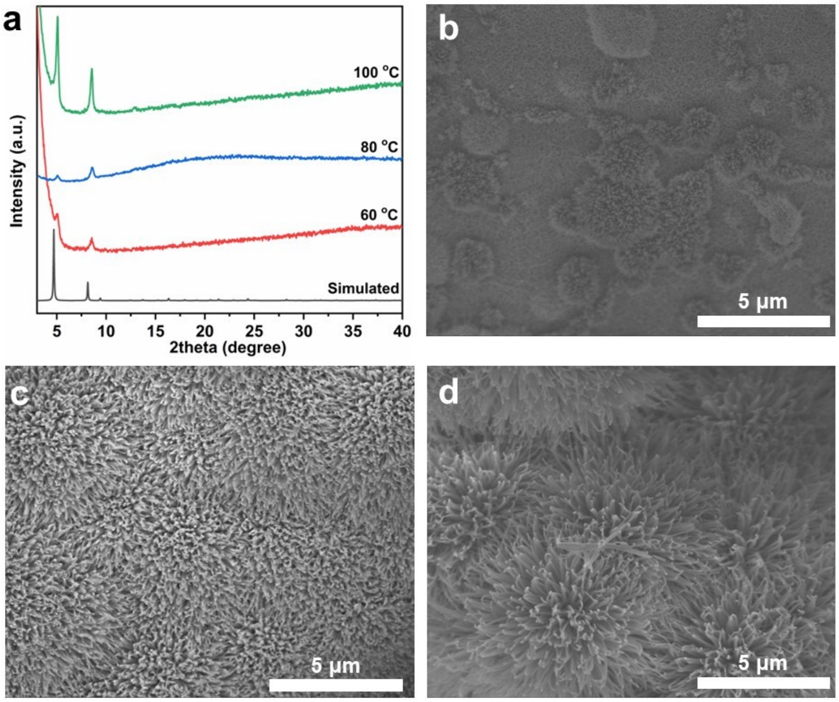

Fig. S8 XRD patterns (a) and SEM images of different reaction temperature, including 60 ^{o}C (b), 80 ^{o}C (c), 100 ^{o}C (d).

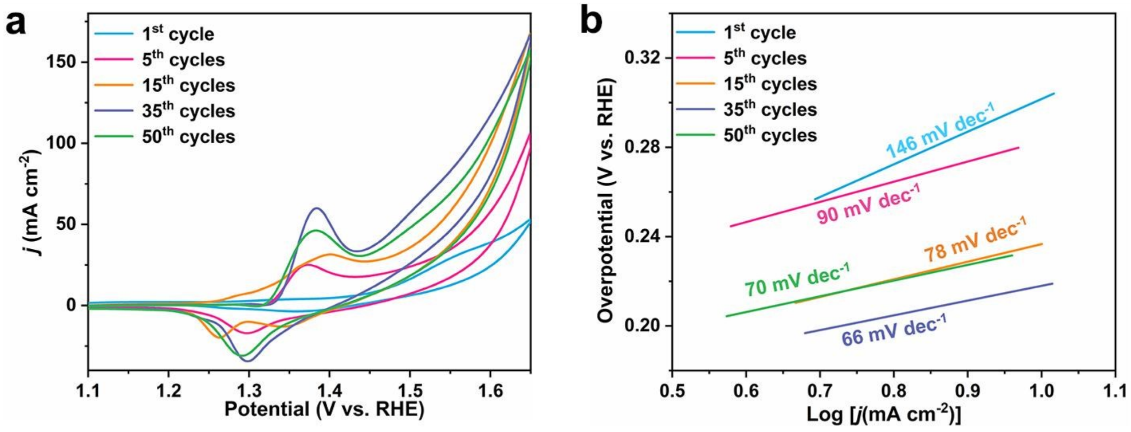

Fig. S9 Electrochemical performance of Ni-BPM/NF-24h. CV curves recorded at a scan rate of 5 mV s^{-1} following various CV cycles which were conducted at 100 mV s^{-1}, between 1.1 and 1.65 V *vs* RHE. (a) and corresponding Tafel slope with the increase of CV cycles (b), respectively.

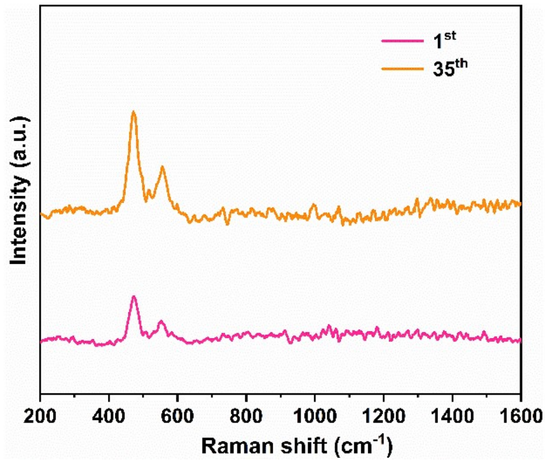

Fig. S10 *In situ* Raman spectra of Ni-BPM/NF-24h during OER process.

Table S2. OER performances of this work and reported MOFs-based electrocatalysts.

MOFs-based electrocatalysts	Overpotential@ 10 mV cm^{-2} (mV)	Tafel slope (mV dec^{-1})	[Ref]
Ni-BPM/NF-24h	218	66	This work
NiFe-BPM/NF-24h	198	43	This work
NiRu$_{0.08}$-MOF	187	40	5
γ-FeOOH/Ni-MOFNA	193	36	6
Ru$_{0.1}$-NiFe-MOF/NFF	197	34.5	7
Ir-Ni-NDC	210	30	8
Ni(Fe)-MOF	227	38.5	9
NiFe-MOFs	230	86.6	10
NiFe-btz/NF	239	44.3	11
NiFe-NPC/NF	240	34	12
MIL-88A/Ni(OH)$_2$-CC	250	46	13
Co$_3$(HITP)	254	86.5	14
Ni–S/MIL-53(Fe)	256	39	15
Fe-MOFs	259	29.1	16
FeNiCu-MOFs	269	61	17
FeCoNi-btz/NF	263	64	18
MCCF/NiMn-MOFs	280	86	19
CoFe-MOF-74	280	56	20
CoZn MOF	287	76.3	21
Ni-DMBD MOF	295	32	22

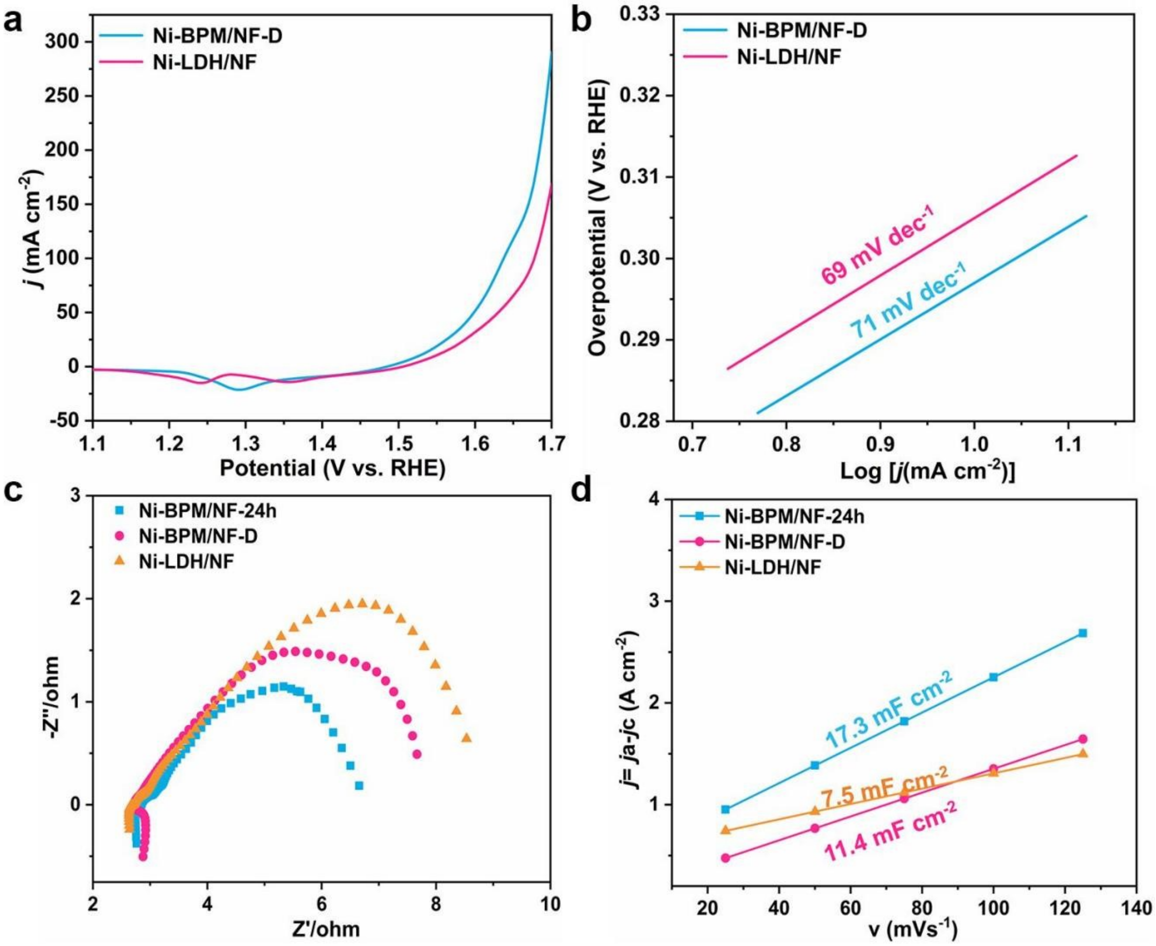

Fig. S11 CV reduction curves recorded at a scan rate of 5 mV s^{-1} (a) and corresponding Tafel slope plots of Ni-BPM/NF-D and Ni-LDH/NF (b). Nyquist plots (c) and C_{dl} curves (d) of Ni-BPM/NF-24h, Ni-BPM/NF-D and Ni-LDH/NF, respectively.

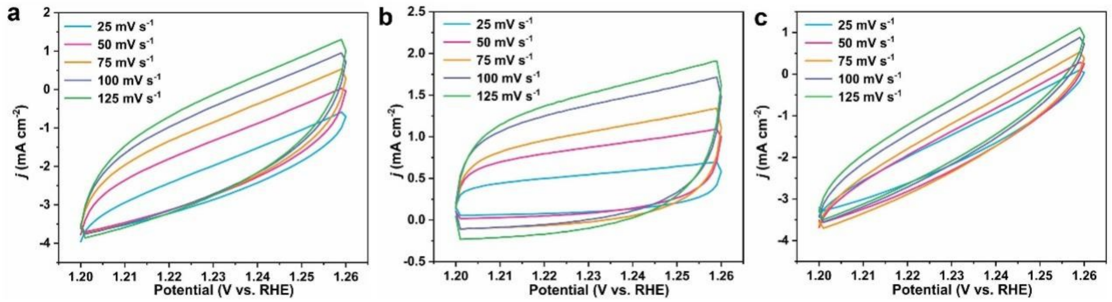

Fig. S12 CV cycles of Ni-BPM/NF-24h (a), Ni-BPM/NF (b) and Ni-LDH/NF (c) in the potential range of 1.2 - 1.26 V *vs* RHE at a scan rate of 50 mV s^{-1}.

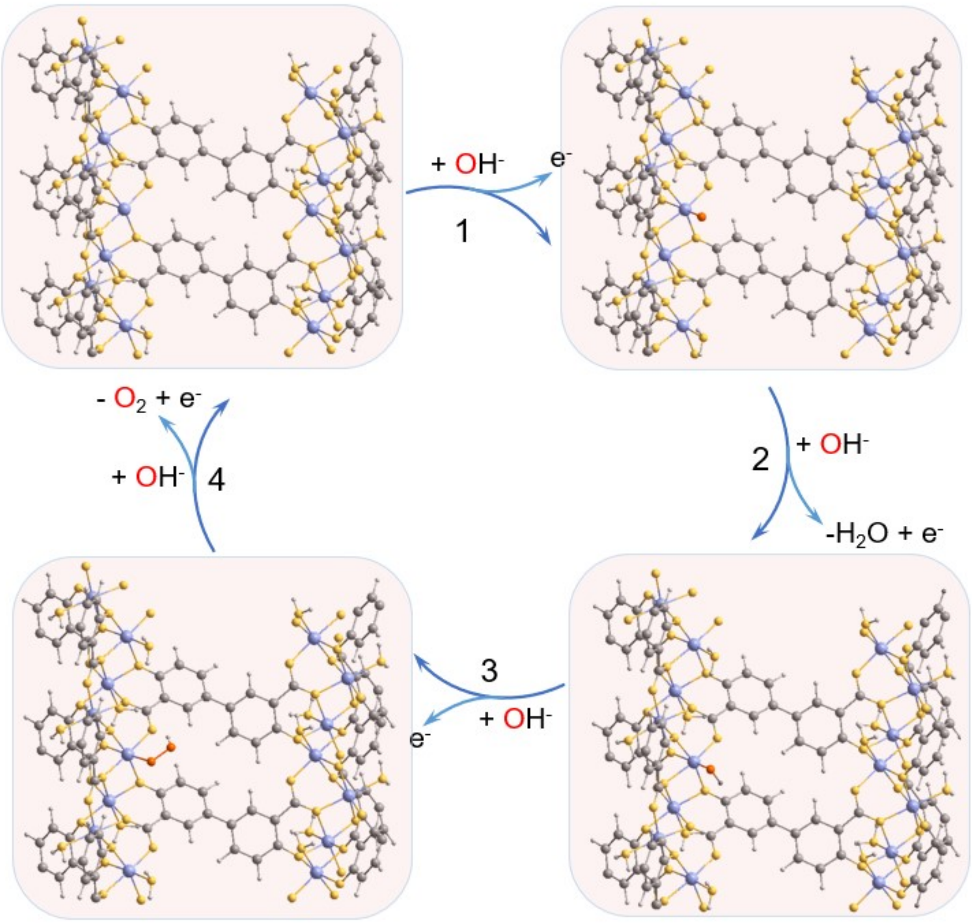

Fig. S13 Illustration of intermediates formation on Ni sites of pristine Ni-BPM.

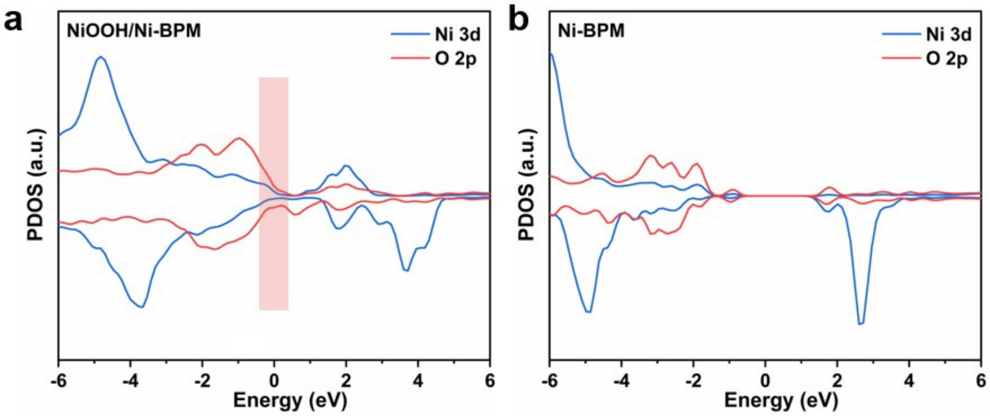

Fig. S14 PDOS plots of Ni 3d and O 2p of *γ*-NiOOH/Ni-BPM (a) and Ni-BPM (b), respectively.

Fig. S15 Optical photographs of the pristine Ni-BPM/NF-24h electrode, electrodes after testing with different CV cycles, and the recovered electrodes.

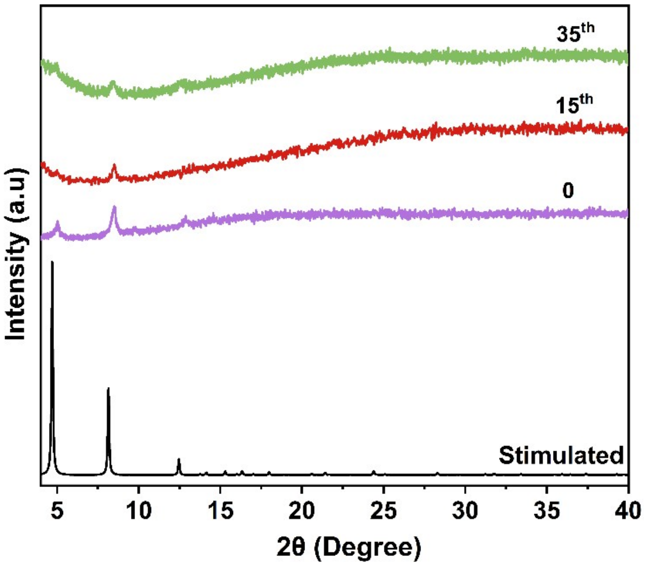

Fig. S16 XRD patterns of simluated Ni-BPM, Ni-BPM/NF-24h and Ni-BPM/NF-24h after 15th and 35th cycle tests.

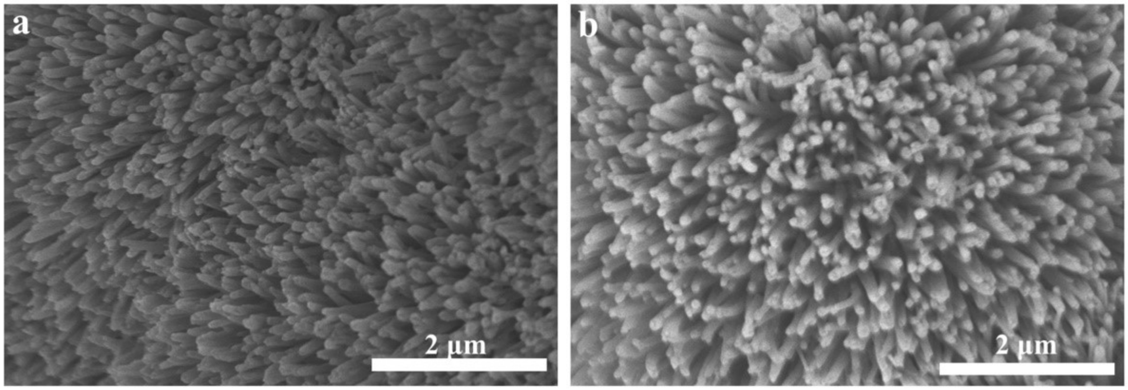

Fig. S17 SEM images of Ni-BPM/NF-24h after 15th (a) and 35th (b) cycles test.

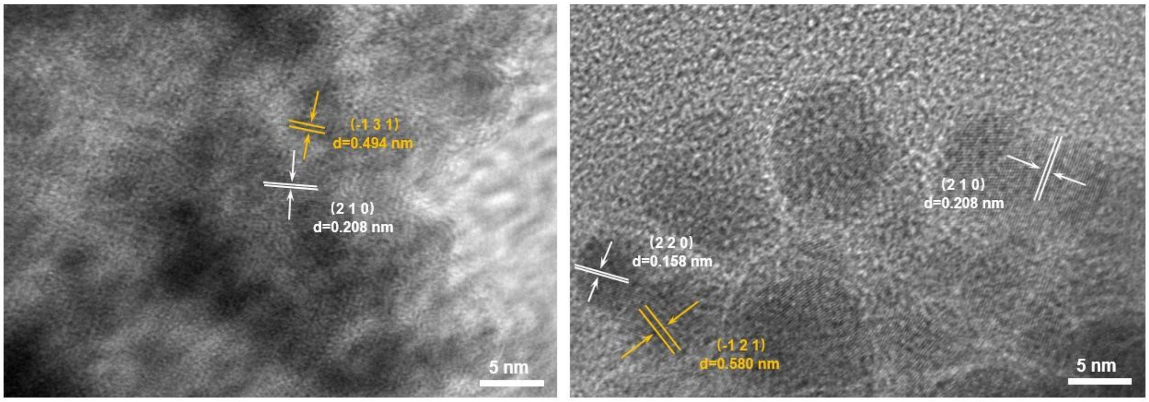

Fig. S18 HRTEM images of Ni-BPM/NF-24h after 15th (a) and 35th (b) cycles test.

Table S3. EXAFS fitting parameters at the Ni *K*-edge for various samples.

Sample	Shell	CN^a	R(Å)^b	σ^2(Å^2)^c	ΔE_0(eV)^d	R factor
Ni foil	Ni-Ni	12*	2.481±0.002	0.0061±0.0003	6.9±0.4	0.0019
NiO	Ni-O	5.9±0.8	2.093±0.014	0.0063±0.0020	4.1±1.5	0.0042
	Ni-Ni	13.5±1.2	2.949±0.006	0.0072±0.0008	0.8±0.9	
Ni-BPM/NF	Ni-O	3.5±0.3	2.035±0.008	0.0062±0.0007	-3.2±0.8	0.0031
	Ni-Ni	5.6±0.5	2.486±0.005			
Ni-BPM/NF-R	Ni-O	3.7±0.3	2.036±0.009	0.0063±0.0009	-3.1±0.9	0.0040
	Ni-Ni	5.2±0.6	2.487±0.005			

^{a}*CN*, coordination number; ^{b}*R*, the distance to the neighboring atom; $^c\sigma^2$, the mean square relative displacement (MSRD); $^d\Delta E_0$, inner potential correction; *R* factor indicates the goodness of the fit. S02 was fixed to 0.829, according to the experimental EXAFS fit of Ni foil by fixing CN as the known crystallographic value. * This value was fixed during EXAFS fitting, based on the known structure of Ni. Fitting range: 2.5 ≤ k (/Å) ≤ 12.0 and 1.0 ≤ R (Å) ≤ 3.0 (Ni foil); 3.2 ≤ k (/Å) ≤ 12.0 and 1.0 ≤ R (Å) ≤ 3.2 (NiO); 2.5 ≤ k (/Å) ≤ 12.0 and 1.0 ≤ R (Å) ≤ 2.6 (Ni-BPM/NF); 2.5 ≤ k (/Å) ≤ 12.0 and 1.0 ≤ R (Å) ≤ 2.6 (Ni-BPM/NF-R). A reasonable range of EXAFS fitting parameters: 0.700 < S02 < 1.000; CN > 0; σ2 > 0 Å2; |ΔE0| < 15 eV; R factor < 0.02.

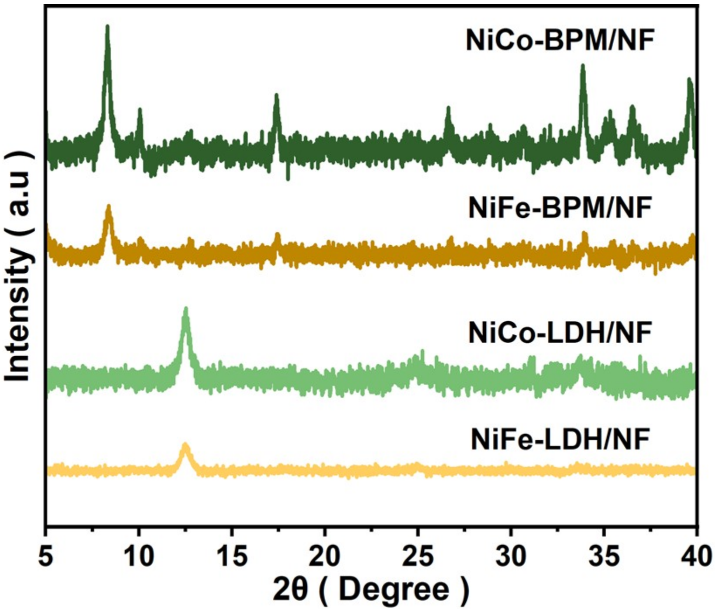

Fig. S19 XRD patterns of NiFe-LDH/NF, NiCo-LDH/NF, NiFe-BPM/NF and NiCo-BPM/NF, respectively.

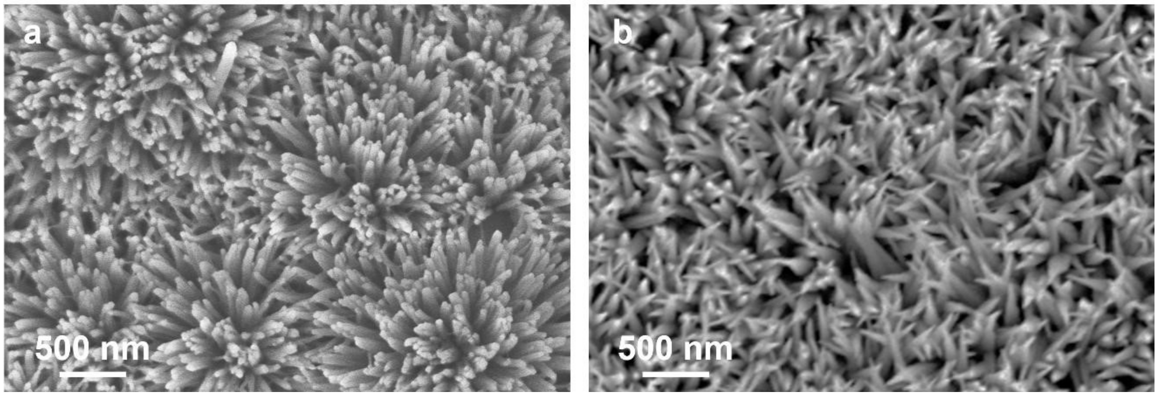

Fig. S20 SEM images of NiFe-BPM/NF (a) and NiCo-BPM/NF (b).

Table S4 The element percentages in NiFe-BPM/NF and NiCo-BPM/NF from ICP-OES analysis.

Mass ratio	NiFe-BPM/NF	NiCo-BPM/NF
Ni：M (M = Fe or Co)	1 : 0.49	1 : 0.12

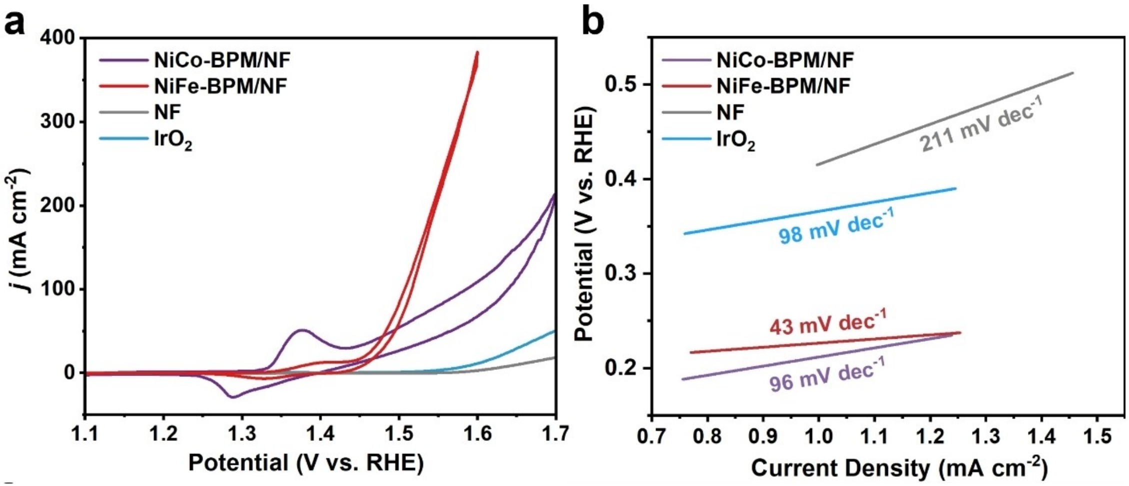

Fig. S21 CV curves at 5 mV s^{-1} of NiFe-BPM/NF, NiCo-BPM/NF and LSV curves at 5 mV s^{-1} of IrO_2, NF (a) and Tafel plots (b) of NiFe-BPM/NF, NiCo-BPM/NF, IrO_2 and NF, respectively.

Reference

[1] Kresse G, Furthmuller J, *Physical Review B* 1996; 54, 11169.

[2] Norskov J. K, Rossmeisl J, Logadottir A. et al. Phys. Chem. B 2004; 108, 17886.

[3] Kulkarni A, Siahrostami S, Patel A. et al. *Chem. Rev.* 2018; 118, 2302.

[4] Wang V, Xu N, Liu J. C. et al. *Comput. Phys. Commun.* 2021; 267, 108033.

[5] Li Y, Wu Y, Li T. et al. *Carbon Energy* 2022; 4, 1076.

[6] Ni C, Zheng H, Liu W. et al. *Adv. Funct. Mater.* 2023; 33, 2301075.

[7] Jiang W, Wang J, Jiang Y. et al. *J Mater. Chem. A* 2023; 11, 2769.

[8] Yang J, Shen Y, Sun Y. et al. *Angew Chem Int Ed Engl* 2023; 62, e202302220.

[9] Cao C, Ma DD, Xu Q, Wu XT, Zhu QL. *Adv. Funct. Mater.* 2018; 29, 1807418.

[10] Ji Q, Kong Y, Wang C. et al. *ACS Catal.* 2020; 10, 5691.

[11] Li S, Wang T, Tang D. et al. *Adv. Sci.* 2022; 9, e2203712.

[12] Jiao L, Wei W, Li X. et al. *Rare Metals* 2022; 41, 3654.

[13] Qian Z, Wang K, Shi K. et al. *J Mater. Chem. A* 2020; 8, 3311.

[14] Xing D, Wang Y, Zhou P. et al. Appl. Catal. B: Environ., 2020; 278, 119295.

[15] Wu F, Guo X, Hao G, Hu Y. et al. *Nanoscale* 2019;11, 14785.

[16] Zhao X,.Wang S, Cao Y, Li Y. et al. Adv. Sci. 2024, 2405936.

[17] Zhai Q, Hu K, Shi Y. H. et al. *J Phys. Chem. Lett.* 2023; 14, 1156.

[18] Lin C, Li J, Li, X. et al. *Nat. Catal.* 2021; 4,1012.

[19] Cheng W, Lu XF, Luan D, Lou XWD. *Angew Chem Int Ed Engl* 2020; 59, 18234.

[20] Zhao X, Pattengale B, Fan D. et al. ACS Energy Lett. 2018; 3, 2520.

[21] Wu J, Yu Z, Zhang Y. et al. *Small* 2021;17, e2105150.

[22] Liu Y, Li X, Zhang S. et al. *Adv. Mater.* 2023; 35, e2300945.